EPJ Web of Conferences **140**, 07007 (2017) DOI: 10.1051/epjconf/201714007007
Powders & Grains 2017

A spheropolygonal-based DEM study into breakage under repetitive compression

Guien Miao[1,*], *Fernando* Alonso-Marroquin[1], and *David* Airey[1]

[1]School of Civil Engineering, The University of Sydney, NSW Australia 2006

Abstract. Experimental breakage studies have often focused on comparing grading and particle shape data from the beginning and end of a test, but one major advantage of DEM simulations is that, although the data are still discrete, more information on intermediate stages is available. This paper describes a repetitive compression test using a 2D aggregate-based DEM model comprised of spheropolygonal particles (formed by the Minkowski sum of a circle and a polygon, viz. sweeping a circle around the edges of the polygon) that are connected by beams and compares the behaviour with experimental data on the breakage of Barrys Beach carbonate sand. The one-dimensional repetitive compression test was performed on 20 particles—each consisting of over 100 sub-particles—which were generated from the outlines of particles of Barrys Beach carbonate sand. Particle breakage was described through the breakage of beams (particle bonds), allowing the evaluation of changes in the compressibility and grading. It was noted that the simulation compared well with the experimental behaviour of Barrys Beach carbonate sand.

1 Introduction

Breakage causes particle shapes to tend away from extremes and particle size distributions to tend towards increasing well-gradedness [1]. Consequently, substantial changes occur to the macroscopic properties—such as density, compressibility and strength—of a soil. Thus, an understanding of how both particle shape and grading evolve as a result of breakage under compression will provide further insight into how the behaviour of a soil will change as a result of very large applied loads.

The Discrete Element Method, DEM, is a discontinuum model that was proposed by Cundall & Strack [2]. The method allows the exploration of the interactions between particles within a granular assembly as the modelling of individual particles within DEM reflects the discrete nature of particles in real granular media, where particles only interact at points of contact. Many DEM studies use circular particles; however, a significant advantage of spheropolygonal particles [3] is that they eliminate the complications associated with the formulation of rolling resistance to account for particle shape when using circular particles. The use of spheropolygons in DEM also offers the opportunity to model a variety of shapes; most significantly, it allows for variation in the angularity of particles away from perfectly round (circular) or perfectly angular (polygonal) particles through the variation of the radius of the circle that is swept around the polygon (spheroradius).

Breakage can be modelled in DEM via using solid-bridge bonds/beams [4]. The bond's properties determine its reaction against imposed forces, giving continuity to the bond behaviour under all relevant deformations: axial, tangential and rotational.

2 Methodology

Repetitive compression involves a number of cycles of monotonic compression with sample reconstitution between cycles. It is a methodology which induces more particle movement than monotonic compression and therefore results in greater amounts of breakage [5]. In this study, experimental and 2D DEM data in the case of repetitive compression is compared to demonstrate the utility of the model in providing data on the breakage behaviour of soils under one-dimensional compression.

2.1 Experimental Repetitive Compression

A uniformly graded sample of Barrys Beach sand weighing 30 g was placed in a one-dimensional compression cylinder with an internal diameter of 35 mm and repetitively compressed to stresses of 95 MPa. A carbonate sand was used in this study as the brittleness and the irregular shape of the particles of carbonate sands [7] allow for a higher amount of breakage for a given load and thus the final state can be reached more quickly. The uniformity of the soil also induces maximal breakage [1].

2.2 DEM Repetitive Compression

A one-dimensional repetitive compression test was performed on 20 particles—each consisting of over 100 sub-particles—which were generated from the outlines of

* Corresponding author: guien.miao@sydney.edu.au

20 particles of Barrys Beach carbonate sand. The DEM model used in this study is a two-dimensional spheropolygonal-based model, shown in Fig 1. The discretisation of each grain is the only source of disorder in this model. The size effects of particle strength are accounted for via the larger particles consisting of more sub-particles and therefore containing a greater number of sites where failure can occur. 2D DEM studies are advantageous in providing qualitative information on the behaviour of granular assemblies without the computational complexity of 3D models [3].

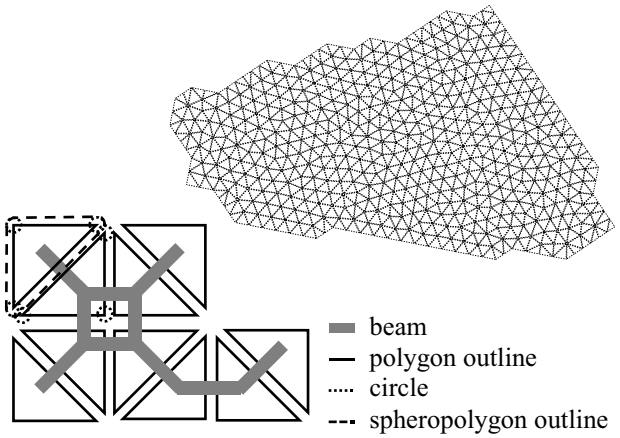

Fig. 1. Example of a triangulated particle with a schematic diagram of a solid-bridge bond (beam) model

Two models were used in this study, a non-convex particle model (as detailed in [3]) and a convex particle model. The non-convex model was used to place the particles without breakage, whilst the convex model was used to model the subsequent breakage of the assembly under compression. The contact forces between two particles, i and j, are described by (1) for the non-convex model and (2) for the convex model.

$$F_c^{ij} = \sum_{k,l} F_{V_{i,k}E_{j,l}} + \sum_{m,n} F_{V_{j,m}E_{i,n}} \quad (1)$$

$$F_c^{ij} = \sum_{k} F_{V_{i,k}P_j} + \sum_{l} F_{V_{j,l}P_i} \quad (2)$$

where $V_{i,k}$ refers to the vertex of particle i with index k, which is in contact $E_{j,l}$, that is, the edge of particle j with index l or in contact with a convex polygonal particle P_j.

The breakage model consists of a contact model and a beam/bond model and the interaction between contact forces and beam forces is described by (3), (4) and (5).

$$\boldsymbol{F_n} = \sum_c (\boldsymbol{F_c^{n,e}} + \boldsymbol{F_c^{n,v}}) + \boldsymbol{F_b} \quad (3)$$

$$\boldsymbol{F_t} = \sum_c \left(\boldsymbol{F_c^{t,e}} + \boldsymbol{F_c^{t,v}}\right) + \boldsymbol{V_b} \quad (4)$$

$$M = \sum_c \boldsymbol{F_n} \times \boldsymbol{r_a} + \sum_c \boldsymbol{F_t} \times \boldsymbol{r_b} + M_b \quad (5)$$

where F_n is the overall normal force, consisting of elastic and viscous components of the contact forces ($F_c^{n,e}$ and $F_c^{n,v}$ respectively) and a beam component (F_b); F_t is the overall tangential force, also consisting of elastic and viscous components of the contact forces ($F_c^{t,e}$ and $F_c^{t,v}$ respectively) and a beam component (V_b); and M is the torque caused by the normal and tangential forces with a beam component (M_b).

Renzo & Di Maio explored different contact models and noted that, on a macroscopic level, the agreement with experimental results was better with a simpler model [7]. For this reason, a relatively simple normal contact model, as described by (6), was used:

$$F_c^{n,e} = \frac{k_n \delta^3}{(\delta - \delta_m) l_c} \quad (6)$$

where k_n is the normal contact stiffness, δ is the overlap between two particles, δ_m is the maximum overlap (which is defined as the sum of the two spheroradii of the particles) and l_c is a characteristic length (which is required for dimensional compatibility and given a nominal value of 1 cm). The contact force is proportional to the area of the contact, which is a function of δ^2, and tends to infinity at $\delta = \delta_m$. It creates adhesive forces at small overlaps with repulsive forces at large overlaps when combined with a simple first-order (Euler-Bernoulli) beam as shown in Fig. 2. The tangential contact model is a standard frictional contact model.

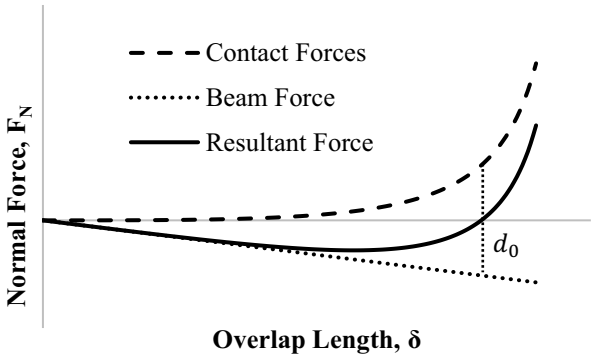

Fig. 2. The normal forces applied to a given sub-particle in the range of $0 \leq \delta_0 \leq 0.9\delta_m$

The failure criterion that governed the breakage of the beams is shown in (7). The criterion was non-linear and allowed breakage only under tension. The criterion reflects the equivalent effect of axial stress on the plastic moment capacity and combined moment and shear failure criterion [9] for the failure of beams.

$$\sqrt{\frac{|M|}{M_f} + \frac{\sigma_p}{\sigma_f} + \left(\frac{\tau_p}{\tau_f}\right)^2} \geq 1 \quad (7)$$

where σ_p and τ_p are the axial (tensile) and shear stresses respectively when projected onto vectors normal and tangential to the failure plane.

3 Compression Curves

Fig. 3 shows a strong similarity between the experimental and DEM compression curves. As the simulation was two-dimensional, a modified definition of void ratio, $e = A_v/A_s$, was used. In both cases, with increasing cycles of compression, the void ratio at high stresses decreases to an asymptotic value and the slope of the limiting compression curve, LCC, (the slope of the compression

curve after yield) becomes less steep with increasing cycles (breakage). In the compression curves from the DEM simulation, it should be noted that the first two cycles are similar as the first cycle was terminated early. While the change in the LCC at early cycles is associated with the occurrence of breakage, the increasing similarity of the final LCCs is an indication of the cessation of breakage.

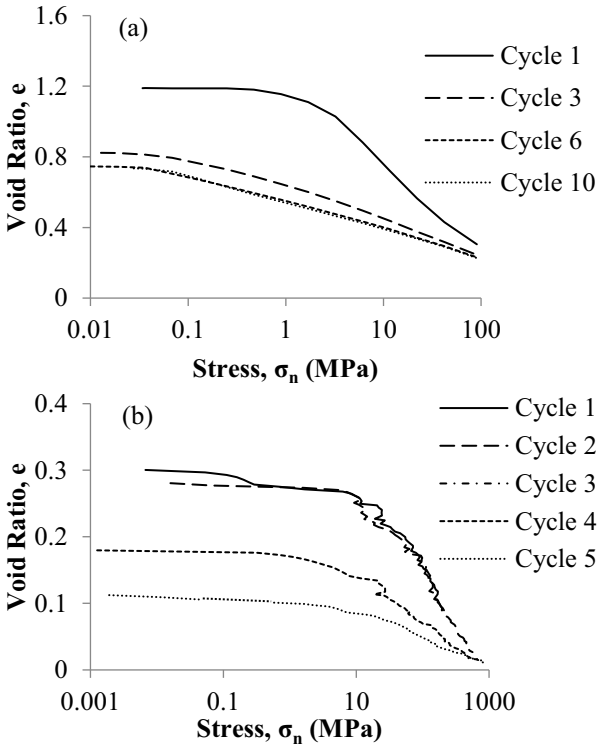

Fig. 3. Compression curves for a repetitively compressed assembly obtained from (a) an experiment and (b) DEM

The stiffness of the material increases with each cycle of repetitive compression. This is due to breakage causing a reduction in particle irregularity and an increasingly well-graded particle size distribution, as can be seen in Fig. 4. Decreasing particle irregularity has been shown by [9] to increase the soil stiffness; it has also been shown that a well-graded sand will have a lower LCC gradient—or equivalently, compression index, C_c—than a uniform grading of the same material [10]. These changes produce a particle assembly which has a greater packing potential so particles are less free to move translationally or rotationally and the assembly therefore becomes stiffer.

Of interest is that the limiting compression curve decreases in slope and begins to reduce in slope at very high stresses (or alternatively, at very low void ratios) in the case of the DEM simulation. This behaviour was not noted in the experimental results due to limitations in the apparatus which did not allow higher stresses to be achieved; however, this behaviour is in line with the expected behaviour of the LCC as it cannot continue infinitely downwards as a void ratio of zero is a limit by definition. Ueda et al. noted similar behaviour in their monotonic compression tests; however, their comminution limit was reached at a significantly higher void ratio [11]. The mean sub-particle diameter used in their study was 10 mm, which is higher than the maximum mesh size of 5 mm size used in this study. It would be expected that the use of a larger minimum particle size would result in the comminution limit being reached at a higher void ratio because the minimum particle size constrains the potential amount of breakage as well as the reduction in void space.

It should also be noted that the void ratios for the simulation lie significantly below the range of void ratios for Barrys Beach sand (e_{min} = 1.25; e_{max} = 1.61). The minimum void ratio for circular (two-dimensional) disks can be shown to be 0.103 by geometry whilst the densest packing of (three-dimensional) spheres is achieved by close-packing, yielding a void ratio of approximately 0.35. Thus, even in ordered assemblies, the transition from 2D to 3D results in a substantial increase in the void ratio. The initial void ratio for DEM simulation is furthermore significantly higher than the minimum void ratio for circular disks due to the irregular particle shapes and particle arrangement. For disordered assemblies of irregular particles, it would be expected that the difference in packing between 2D and 3D void ratios would be greater due to the greater variation in shape allowing a significantly more open structure in three dimensions.

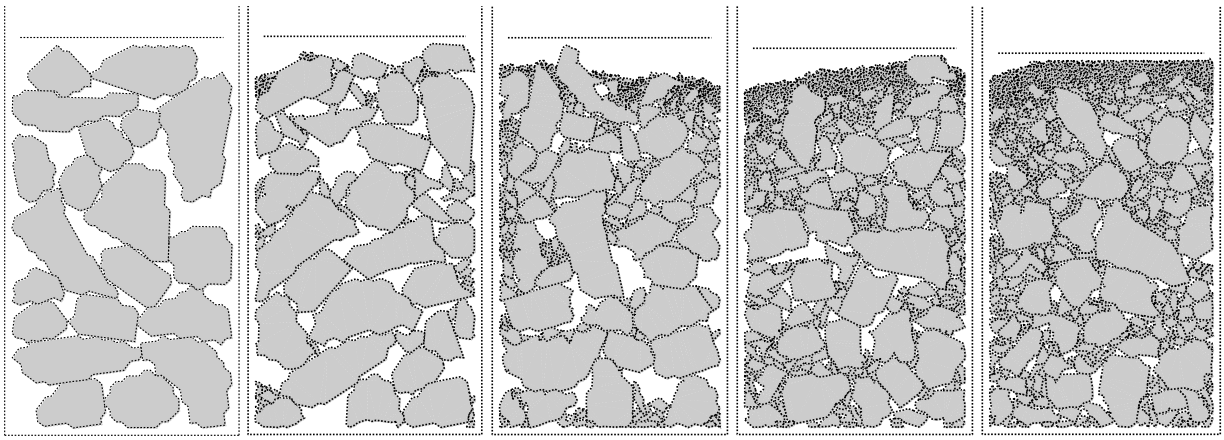

Fig. 4. Visualisation of particle assemblies at the start of each cycle of repetitive compression

4 Grading

Fig. 5 shows the evolving gradings with increasing cycles of breakage for both the experimental and DEM cases. Although the particle sizes produced are not similar (due to limitations in the minimum particle size for the simulation), there are still key similarities between the two sets of data. It can be seen that the greatest amount of breakage occurs within the first cycle and that the difference in grading for later cycles reduces. This occurs in spite of the grading change in first cycle being less than expected due to early termination of the test. This reflects the behaviour of the compression curves shown in Fig. 3, where the greatest changes in void ratio occur in early cycles and differences in later cycles are smaller.

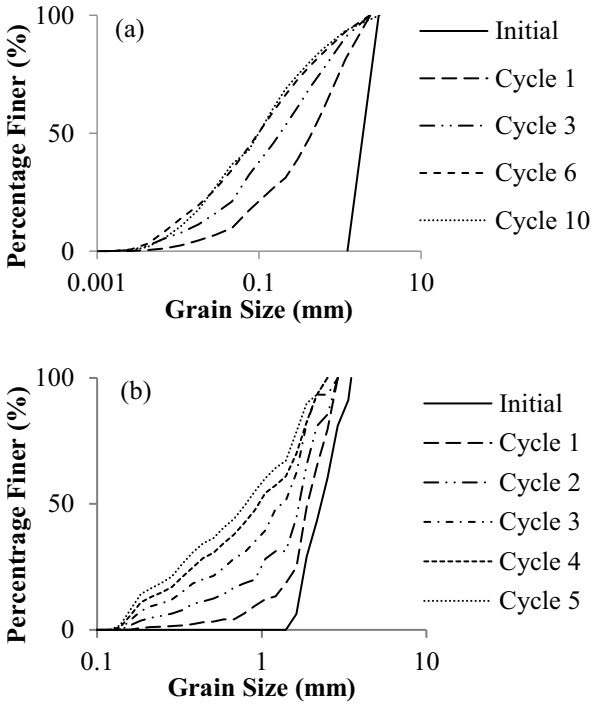

Fig. 5. Evolution of grading for a repetitively compressed assembly obtained from (a) an experiment and (b) DEM

Furthermore, in both cases, the largest particles undergo complete breakage, which confirms the findings of Bridgwater et al. that 100% attrition of particles is possible when using analyses which capture relatively small changes [12]. Nevertheless, there is a difference in the curvature of the experimental and numerical gradings. Although the experimental grading is single-curvature (with no inflection point) after a single cycle, it becomes double-curvature after more cycles. Conversely, the DEM grading remains single-curvature throughout the test, in part due to the complete breakage of the coarsest particles.

Now, Palmer & Sanderson's model suggests that when each grain has an equal probability of fracture, a (single-curvature) mono-fractal particle size distribution evolves [13]. Therefore, the transition from a single-curvature grading to a double-curvature grading suggests that there is an unequal probability of breakage which is skewed towards the breakage of larger particles in the case of the experiment, resulting in preferential breakage of the larger particles. The complete breakage of the coarsest particles in the DEM simulation suggests that there is indeed a preferential breakage of the coarsest particles; however, better particle cushioning in the experimental gradings may have contributed to the protection of the coarsest particles from complete breakage. In fact, it can be seen from Fig. 4 that the particle placement did not result in an even distribution of fines, which may have caused a bias towards greater breakage. The simulation produces gradings that are linear in semi-log scale, which is similar to those from the experiments of Lőrincz et al., who noted a significant loss of fines during their tests [5].

5 Conclusion

As in the experimental data, the compression curves showed an increase in the stiffness of the soil and downward shift with increasing cycles. Furthermore, the grading was also noted to become increasingly well-graded and finer with increasing stress and increasing cycles as in the experiment. Interestingly, in contrast to the experimental data on the Barrys Beach sand, which showed the formation of double-curvature grading, the grading in the simulation tended towards a single-curvature grading that is linear in semi-log space. This may be attributed to insufficient sample-mixing in the DEM simulation and may better reflect situations where fines are lost from the sample during experiments. Despite limitations in the model (2D with only a few particles), the similarities between the simulation and the experimental data demonstrate the utility of the model for a qualitative analysis of breakage behaviour.

References

1. K. Lee, I. Farhoomand, Can. Geotech. J **4**, 1 (1967)
2. P.A. Cundall, O.D.L. Strack, Géotechnique **29**, 1 (1979)
3. F. Alonso-Marroquin, Y. Wang, Granul. Matter **11**, 5 (2009)
4. F. Kun, H.J. Herrmann, Comput. Methods Appl. Mech. Eng. **138**, 1 (1996)
5. J. Lőrincz, E. Imre, M. Gálos, Q.P. Trang, K. Rajkai, S. Fityus, G. Telekes, Int. J. Geomech. **5,** 4 (2005)
6. J.P. Carter, D.W. Airey, M. Fahey, *A Review of Laboratory Testing of Calcareous Soils* (1999)
7. A. Di Renzo, F.P. Di Maio, Chem. Eng. Sci., **59**, 3 (2004)
8. D. Drucker, R. Providence, *The Effect of Shear on the Plastic Bending of Beams* (1955)
9. G.C. Cho, J. Dodds, J.C. Santamarina, J. Geotech. Geoenviron. **132**, 5 (2006)
10. M.R. Coop, Géotechnique **40**, 4 (1990)
11. T. Ueda, T. Matsushima, Y. Yamada, Granul. Matter **15**, 5 (2013)
12. J. Bridgwater, R. Utsumi, Z. Zhang, T. Tuladhar, Chem. Eng. Sci. **58**, 20 (2003)
13. A. Palmer, T. Sanderson, Proc. R. Soc., Lond., Ser. A **433**, 1889 (1991)